◉ISAC CYTOMETRY
INTERNATIONAL SOCIETY FOR ADVANCEMENT OF CYTOMETRY   Journal of Quantitative Cell Science PART A

Phenotypic analysis of the pediatric immune response to SARS-CoV-2 by flow cytometry

Freya Sibbertsen[1] ⓘ | Laura Glau[2] | Kevin Paul[1] ⓘ | Thomas S. Mir[3] ⓘ | Søren W. Gersting[1] ⓘ | Eva Tolosa[2] | Gabor A. Dunay[1] ⓘ

[1]University Children's Research, UCR@Kinder-UKE, University Medical Center Hamburg-Eppendorf, Hamburg, Germany

[2]Institute for Immunology, University Medical Center Hamburg-Eppendorf, Hamburg, Germany

[3]Department of Pediatric Cardiology, University Medical Center Hamburg-Eppendorf, Hamburg, Germany

Correspondence

Gabor A. Dunay, University Children's Research, UCR@Kinder-UKE, University Medical Center Hamburg-Eppendorf, Martinistraße 52, Hamburg 20246, Germany.
Email: g.dunay@uke.de

Abstract

Pediatric SARS-CoV-2 infection is often mild or asymptomatic and the immune responses of children are understudied compared to adults. Here, we present and evaluate the performance of a two-panel (16- and 17 parameter) flow cytometry-based approach for immune phenotypic analysis of cryopreserved PBMC samples from children after SARS-CoV-2 infection. The panels were optimized based on previous SARS-CoV-2 related studies for the pediatric immune system. PBMC samples from seven SARS-CoV-2 seropositive children from early 2020 and five age-matched healthy controls were stained for analysis of T-cells (panel T), B and innate immune cells (panel B). Performance of the panels was evaluated in two parallel approaches, namely classical manual gating of known subpopulations and unbiased clustering using the R-based algorithm PhenoGraph. Using manual gating we clearly identified 14 predefined subpopulations of interest for panel T and 19 populations in panel B in low-volume pediatric samples. PhenoGraph found 18 clusters within the T-cell panel and 21 clusters within the innate and B-cell panel that could be unmistakably annotated. Combining the data of the two panels and analysis approaches, we found expected differentially abundant clusters in SARS-CoV-2 seropositive children compared to healthy controls, underscoring the value of these two panels for the analysis of immune response to SARS-CoV-2. We established a two-panel flow cytometry approach that can be used with limited amounts of cryopreserved pediatric samples. Our workflow allowed for a rapid, comprehensive, and robust pediatric immune phenotyping with comparable performance in manual gating and unbiased clustering. These panels may be adapted for large multi-center cohort studies to investigate the pediatric immune response to emerging virus variants in the ongoing and future pandemics.

KEYWORDS

B-cells, children, COVID-19, innate cells, PhenoGraph, SARS-CoV-2, T-cells, UMAP

1 | INTRODUCTION

The current SARS-CoV-2 pandemic has been responsible for over five million deaths by the time of this submission. A total of 10%–20% of adult patients develop a severe or life threatening disease [1]. The majority of children, however, develop mild symptoms, and their contribution to spreading SARS-CoV-2 remains unclear [2, 3]. Immune responses of children to SARS-CoV-2 after illness or asymptomatic infection remain understudied compared to adults, and the understanding of how their immune system clears the virus without resulting in excess inflammation could provide clues for treatment of adult patients [4]. However, children rarely do develop the Multisystem Inflammatory Syndrome in Children (MIS-C) as a secondary consequence of a SARS-CoV-2 infection [5, 6]. Furthermore, the study of long-term immunological changes several months after infection could provide important insights for the rational planning of vaccination efforts for children of different age.

Here, we present an approach to rapidly analyze the frequencies of lymphoid and myeloid cell populations, and the differentiation stages of lymphocytes in pediatric samples of peripheral blood mononuclear cells (PBMC) using two multicolor flow cytometry panels. Our aim was to establish and evaluate panels with a robust performance in classical gating as well as state-of-the art flow bioinformatic approaches such as unbiased clustering and visualization by Uniform Manifold Approximation and Projection analysis (UMAP). Since most broadly available cytometers and commercial fluorochromes limit flow cytometry panels to less than 20 markers, two different panels were designed. The goal of panel T was to identify key functional subsets and differentiation stages of T-cells. Panel B included markers for B-cell subpopulations and for innate cell subsets. The panels have been tailored to target subpopulations with higher relevance in children, such as recent thymic emigrants (RTE) and innate lymphoid subsets, while also considering alterations described for SARS-CoV-2 and other respiratory infections [5–10]. Furthermore, the panels have been developed and optimized for cryopreserved samples, making transport and remote analysis of specimens possible for larger pediatric cohorts in multi-center settings.

2 | PATIENTS AND METHODS

2.1 | Patients

Preliminary titration of antibodies and test stainings were carried out using anonymous buffy coats of adult blood donors from the Department of Transfusion Medicine at the University Medical Center Hamburg-Eppendorf, after their written informed consent . Pediatric blood samples were obtained between May and July of 2020 through the COVID-19 Child Health Investigation of Latent Disease (C19. CHILD) Hamburg Study, registered at clinicaltrials.gov (NCT04534608). Seroconverted children were identified by two independent serum antibody tests in a screening blood sample. The tests targeted the viral nucleocapsid and the S1 and S2 subunits of the viral spike protein using the Elecsys® Anti-SARS-CoV-2 (Roche) and the LIAISON® SARS-CoV-2 serological test (DiaSorin) respectively.

Healthy controls were selected based on a negative SARS-CoV-2 PCR test and negative results in both antibody screening tests. Parents provided written informed consent. Seropositive children were recalled at their convenience for a follow-up visit where PBMC samples were obtained. Since presentation times after recall were variable, serologic testing including quantitative serologies were repeated at the time of PBMC sampling to confirm persistent seropositivity and limit inconsistencies based on time since infection. This data as well as age and gender distribution in the seropositive and control groups are shown in Supplementary Table 3. The study was approved by the local ethical committee of Hamburg (reference number: PV7336).

2.2 | Cryopreservation and thawing of PBMC samples

Blood samples were drawn into EDTA tubes by skilled pediatric phlebotomists and processed within 24 hours. PBMC were isolated using SepMate tubes (StemCell) by gradient centrifugation according to the manufacturer's instructions. PBMCs were cryopreserved in freezing medium containing 50% FBS, 30% RPMI and 20% DMSO and stored in liquid nitrogen until further analysis.

For analysis, frozen aliquots of PBMC were incubated for 1 min in a 37°C water bath, then rapidly thawed in 37°C RPMI by gentle pipetting. Viability was above 80% in all samples.

2.3 | Flow cytometry

Cells were washed twice, and the final staining volumes were adjusted to 100 μl . Each aliquot was stained with a 1:2000 dilution of the Fixable Near-IR Dead Cell Stain Kit (Invitrogen) and incubated for 15 min in the dark. Subsequently, cells were stained with a cocktail of antibodies for Panel T ("T-cells") or Panel B ("B and innate cells"); see Supplementary Tables 1 and 2 for complete composition of antibody cocktails. Optimal staining concentrations per 100 μl staining volume had been determined for each antibody in preliminary experiments by titration (see Supplementary Material "Titration of fluorescent-conjugated antibodies" and Supplementary Figure 1). Cells were incubated with the antibodies for 20 min at room temperature and washed with PBS. Samples were subsequently fixed in 0.75% paraformaldehyde (PFA). PFA was washed off after 1 hour, cells were resuspended in 100 μl PBS and kept at 4°C until analysis.

Sample acquisition was carried out on a BD FACSymphony A3 flow cytometer, using FACS Diva Version 9.1. The instrument configuration is indicated in the Supplementary Material "MIFlowCyt". Single stained compensation beads were used for automatic compensation of the panels in the FACS Diva software: Anti-Mouse or Anti-Rat Ig, κ/Negative Control Compensation Particles Set, BD Biosciences for antibodies, ArC™ Amine Reactive Compensation Bead from Invitrogen for the Dead Cell Stain Kit. Consistency of fluorescence signals between experiments was ensured using Rainbow Calibration Particles (BD Sphero).

2.4 | Data analysis

Data were exported from FACS Diva in the form of .fcs files and further postprocessing and manual gating was carried out using FlowJo Version 10.7.1. The FlowJo Plugin FlowAI was used with default settings for initial cleanup of data. The gating strategy for different cellular subsets is discussed in Results and Discussion. Visualization of the multidimensional data was performed using the dimensionality reduction algorithm Uniform Manifold Approximation and Projection (UMAP), provided in the R-package "umap". For each panel a dataset containing the same number of events from each of the two groups (in total 300,000 CD3+ cells for panel T and 300,000 CD45+CD3- cells for panel B from seroconverted and healthy control children) was randomly chosen. Before analysis, the files from both groups were concatenated panelwise to obtain comparable visualizations and sets of clusters. T-cells were excluded from panel B for better assessment of low abundant cell subsets. In order to reduce sample-to-sample acquisition variability, we applied the "gaussNorm" normalization algorithm from the R-package "flowStats" prior to UMAP and clustering. For unbiased determination of clusters, the algorithm PhenoGraph was run on CD45+CD3- cells and CD3+ cells for panel B and panel T, respectively, using the R-package "cytofkit" [11] with default parameters except for parameter k-nearest neighbors which was set to 150 to yield clusters containing 1%–25% of the analyzed events in each panel. The parameters CD45-BUV396, CD3-BV786 and LiveDead NIR (APC-Cy7) were excluded from the cluster analysis. This setting generated 18 clusters for panel T and 23 clusters for panel B. The resulting clusters were projected onto the UMAP representation and annotated for the different cell types or cell states according to lineage marker expression (Supplementary Figures 2 and 3).

2.5 | Statistical analysis

Data analysis was performed with Microsoft Excel (Microsoft Office 365) and GraphPad Prism 8 (GraphPad Software Inc., San Diego, California) and RStudio (Version 1.4.1717). Statistical analysis was performed on manually gated subpopulations and computationally detected cell clusters of CD3+ (Panel T) and CD45+CD3- (Panel B) populations using unpaired t-test (2-tailed). Bonferroni correction for multiple testing was applied to all statistical analysis.

3 | RESULTS AND DISCUSSION

3.1 | Gating and interpretation of panel T for T-cells

After gating of single lymphocytes and exclusion of dead cells, CD3 positive cells were identified (Figure 1A). This was followed by separation of γδ T cells (TGD). During the first SARS epidemic γδ T effector memory cells were expanded approximately 3 months post symptom onset in seroconverted adult patients, and had a protective role by killing SARS-CoV–infected target cells [12].

Within classical T-cells, CD4 and CD8 lineages were gated within the TCR-γδ negative CD3 positive population. Regulatory T-cells (Treg) were defined as CD25+CD127low in the CD4 T-cell compartment, as this phenotype correlates well with intracellular staining for FOXP3 [13]. After the exclusion of Treg, CD45RA and CD27 were sufficient in conventional (non-Treg) CD4+ T-cells to distinguish between central memory (Tcm), effector memory (Tem) and naive (Tn). We used CD27 instead of CCR7, because of the similar expression patterns of the two molecules [14] and instability of CCR7 in cryopreserved samples [15]. The coexpression of CD31 and CD45RA on CD4+ conventional T-cells was used to mark recent thymic emigrants (RTE), a large subpopulation in young children [16].

Functional subsets of CD4+ T helper cells were identified on non-naive cells according to the expression of the chemokine receptors CXCR3, CXCR5, and CCR6, the fractalkine receptor CX3CR1, as well as Programmed cell death protein 1 (PD-1). We first defined Th1 (CXCR3+CCR6-), Th17 (CXCR3-CCR6+) and Th1-17 (CXCR3+CCR6+) cells. Cytotoxic CD4+ T-cells were identified as CD28 negative and CX3CR1 positive [17]. T follicular helper cells (Tfh) were identified as CXCR5 positive [18] in CD4+ T-cells.

Apart from the classical paradigm of CD8 naive-effector memory gating [19] (Figure 1A), Panel T allowed for identification of T memory cells expressing the fractalkine receptor CX3CR1 [20]. CD8+ naive and memory subsets (naive Tn, central memory Tcm, transitional memory Ttm, effector memory Tem, terminally differentiated effector Tte) were identified based on expression of CD27, CD45RA, and CD28 [19] as shown in Figure 1A. Furthermore, we identified three populations of cells within the CD8+ subset using CX3CR1 and CD27, namely CX3CR1-CD27+, CX3CR1+CD27dim, CX3CR1+CD27-. By combining the two gating strategies we demonstrated that in pediatric PBMC CX3CR1 expression is mostly restricted to CD28- cells (effector memory and terminally differentiated effector cells) and is lacking in Tcm and naive subsets (Figure 1A).

In a recent study, CX3CR1+CD8+ T-cells (termed "vascular patrolling T-cells") correlated with the need for circulatory support through vasoactive medication in pediatric patients affected by MIS-C associated with SARS-CoV-2 infection, thereby underlining the role of these cells in vascular pathology and the current pandemic [5].

Panel T allows for the analysis of the coinhibitory receptor PD-1 and the chronic activation marker HLA-DR (Figure 1A). Children with SARS-CoV-2 infection show similar viral loads as adults in nasopharyngeal samples [21], but their symptoms are much less pronounced [2], suggesting lower immune activation. PD-1 is associated with more efficient viral clearance and is known to regulate the development of immunologic memory in CD8+ T-cells after respiratory infections [9]. Counter regulation by co-inhibitory receptors, for example, PD-1 among others has been associated with clonal T-cell responses in SARS-CoV-2 infection of adults [8].
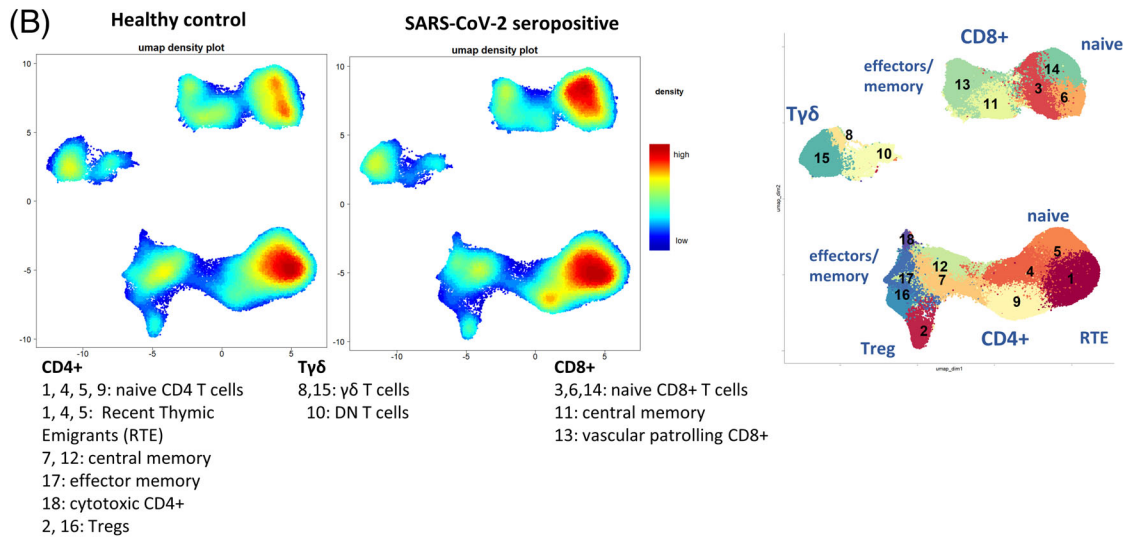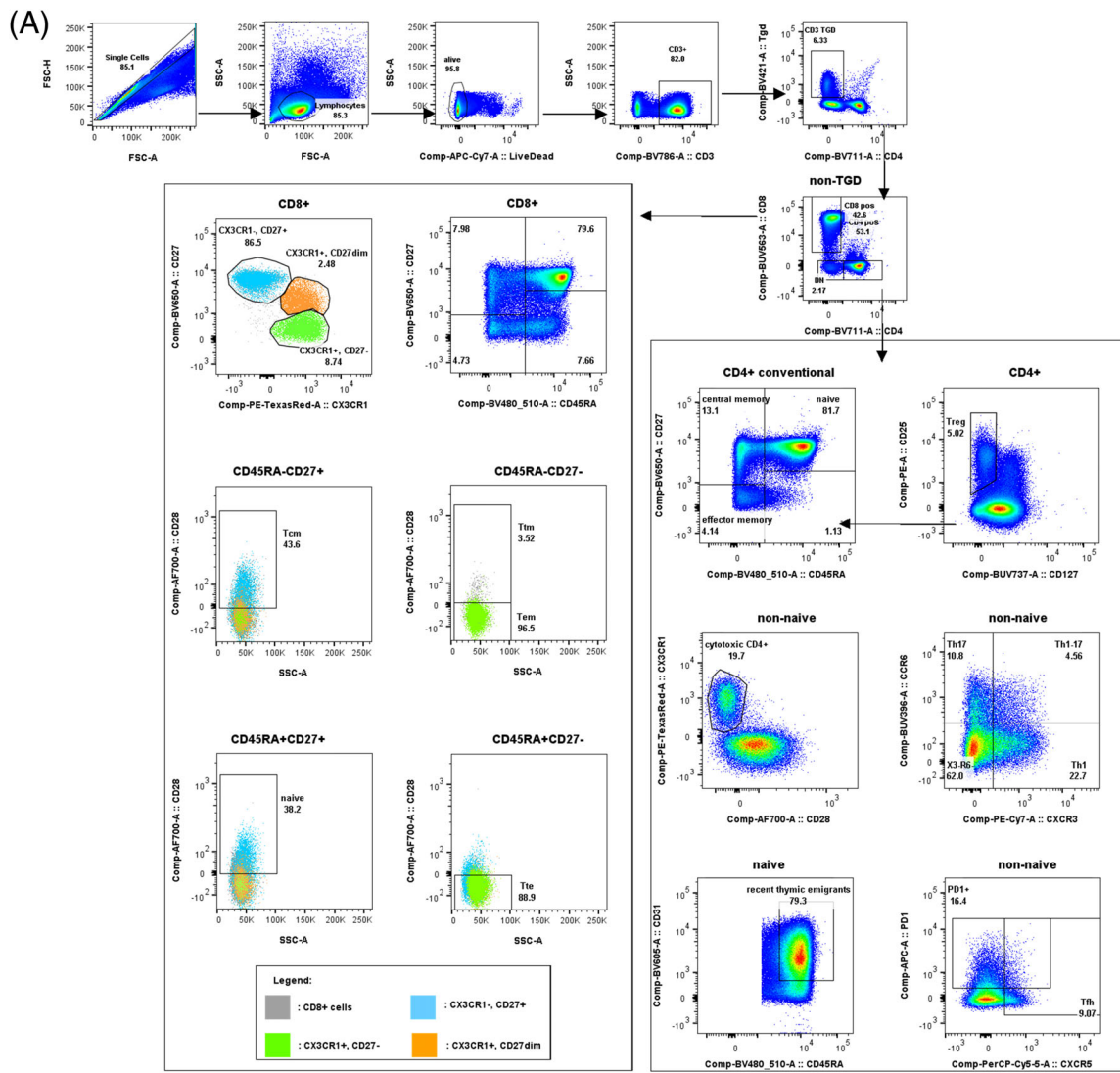
FIGURE 1 Manual gating strategy, and visualization of the unbiased clustering of single-cell multidimensional data for panel T. (A) Manual gating strategy for T-cell subpopulations on a representative sample. Names of subpopulations are shown along with frequency within the parent population. The parent population is indicated above the plots or by arrows showing backgating. Legend: Gray: CD8+ cells; Blue: CX3CR1 negative, CD27 positive cells; Orange: CX3CR1 positive, CD27dim cells; Green: CX3CR1 positive, CD27 negative cells. (B) UMAP analysis of 150,000 live CD3+ lymphocytes per group from SARS-CoV-2 seroconverted children compared to age-matched controls. Density plots showing the UMAP analysis for each group. Populations were manually annotated after unbiased clustering; the annotation is shown below the figure. Healthy controls: $n = 5$; SARS-CoV-2 seropositive $n = 7$

3.2 | Gating and interpretation of panel B for B-cells and innate immune cells

Panel B has been designed based on OMIP-062 [22]. A clean population of PBMCs was obtained by sequential gating of CD45+ events, elimination of doublets and selection of live cells (Figure 2A). To facilitate the visualization of rare cell subpopulations, CD3+ T-cells were excluded from the analysis in this panel.

Basophils and plasmacytoid dendritic cells (pDC) were identified by a high expression of CD123 and their differential expression of HLA-DR.

B-cells were gated based on CD19 expression. The CD19+ B-cell population was further subdivided by their unique expression of surface IgD molecules into mantel zone-like B-cells (CD27+IgD+), naive B-cells (CD27-IgD+) and plasmablasts (IgD-CD27±CD38+).

CD19 negative cells were separated as HLA-DR positive, containing the rest of the myeloid cells, and HLA-DR negative (lymphoid). In the HLA-DR+ subpopulation, classical (CD14+CD16-) and non-classical monocytes (CD14-CD16+) were identified based on the expression of CD14 or CD16. After exclusion of monocytes, a high expression of HLA-DR and intermediate expression of CD123 allowed for identification of a subset of myeloid dendritic cells (mDC).

In the lymphoid subpopulation, CD127 low and positive cells were gated. CD127 low NK cells, and their subsets (CD56 bright, CD56 dim, CD56 negative) were identified by plotting CD16 against CD56. From the CD127+ cluster, the CD127 high and CD161 positive cells were identified as innate lymphoid cells (ILCs), which were further subdivided into functional subsets. CD294, also known as CRTH2, is exclusively expressed by ILC2s, while CD117/c-kit expression identifies ILC3s. Finally, ILC1s are identified by the lack of expression of both markers (CD117-CD294-) [23].

3.3 | UMAP projection and clustering of peripheral blood mononuclear cells

The PhenoGraph analysis generated 18 clusters for panel T (Figure 1B) and 23 clusters for panel B (Figure 2B). In panel T (Figure 1B), we identified several clusters of CD4+ and CD8+ T-cells, as well as three clusters of CD4 and CD8 double negative (DN) cells of which two (clusters 15 and 8) were highly positive for the γδ T-cell receptor. CD8+ T-cells could be divided into naive (clusters 3, 6 and 14) and effector/memory cells (clusters 11 and 13). In the CD4 compartment, we could annotate naive T-cells and recent thymic emigrants (clusters 1, 4, 5, and 9), central memory (clusters 7 and 12), effector/effector memory cells (clusters 17 and 18), and Treg (clusters 2 and 16). T-cell effector subpopulations such as Th1, Th17, Th1-17, and Tfh were not present as a distinct cluster, probably due to small cell numbers in these pediatric samples, even though they were distinctly identified by manual gating (Figure 1A). Importantly, CX3CR1 positive cells presented as a distinct cluster among both CD4 and CD8 effector cells and could thus be annotated as cytotoxic CD4+ (cluster 18) and CX3CR1 positive CD8+ cells (cluster 13) (see also

Supplementary Table 4). Interestingly, PhenoGraph found four naive CD4 T-cell clusters (clusters 1, 4, 5, and 9) differing in their CD31, CD45RA and CD28 expression intensity and two Treg clusters (clusters 2 and 16) differing in their HLA-DR expression intensity. We identified two clusters representing central memory phenotype (clusters 7 and 12), with cluster 12 having a more intense expression of CXCR3, suggesting Th1 cells as part of this cluster. In the CD8 T-cell population we identified three naive T-cell clusters (clusters 3, 6, and 14) differing in their expression intensity of CD127.

In panel T, comparison of seropositive and healthy children revealed no statistical differences in either the unbiased PhenoGraph analysis or the manual gating (Supplementary Figures 4 and 6, Supplementary Table 4). Within CD4 cells, cluster 9 in the PhenoGraph analysis, a part of the naive cell clusters (clusters 1, 4, 5, and 9, Supplementary Figure 6), was slightly increased in seropositive children (Supplementary Figure 6, Supplementary Table 4). This trend was not observed in the overall CD4 naive cell population via manual gating (Supplementary Figure 4, Supplementary Table 4).

In panel B (Figure 2B), we identified basophils (cluster 18), plasmacytoid dendritic cells (pDC, cluster 12), non-classical CD16+ (cluster 10) and classical monocytes (clusters 2 and 11). Both clusters representing the classical monocytes only differ minimally in their expression intensity of HLA-DR, and CD38. Based on high expression of HLA-DR and the lack of CD16 and other linage markers, cluster 9 was annotated as conventional dendritic cells [24]. We identified 7 clusters of different NK cell subpopulations, a heterogeneity that could not be resolved in the manual analysis. The five CD56dimCD16+ NK cell clusters (clusters 5, 13, 16, 20, and 23) differ in their CD161 and CD38 expression intensity (Supplementary Table 5). Two clusters were annotated as innate lymphoid cells (ILC): Cluster 17, including ILC type 1 (ILC1) and ILC type 2 and cluster 22, marking ILC3 (c-kit+). The small size of these populations did not allow for the discrimination of ILC1, for which no positive marker is known, and ILC2, identified clearly in the manual analysis by the expression of CRTH2 (CD294). Among B-cells, we found separate clusters for naive (cluster 3), transitional-(cluster 8), and mantle-zone-like B-cells (cluster 1). Plasmablasts are represented in cluster 7, while cluster 21 represents memory B-cells. Clusters 6 and 14, containing less than 1% of the CD45 + CD3- events, could not be annotated with the markers used. Importantly, 99.03% of the events could be resolved and confidently annotated. Manual gating resolved on average more than 97% of the live population.

In panel B, the frequencies of the different subpopulations were similar when analyzed using manual gating or unbiased clustering by PhenoGraph. pDCs, basophils and IgD-negative B-cells were reduced in seroconverted children compared to healthy controls in the PhenoGraph analysis (cluster 12; Supplementary Figure 7, Supplementary Table 5) as well as in the manual gating analysis (pDC; Supplementary Figure 5, Supplementary Table 5) [25]. In contrast, the frequency of total NK cells was slightly increased (Supplementary Figures 5 and 7, Supplementary Table 5). Interestingly, the frequency of pDC and basophils in the blood of acutely SARS-CoV-2 infected children were also reduced [6], so that in light of our preliminary findings,
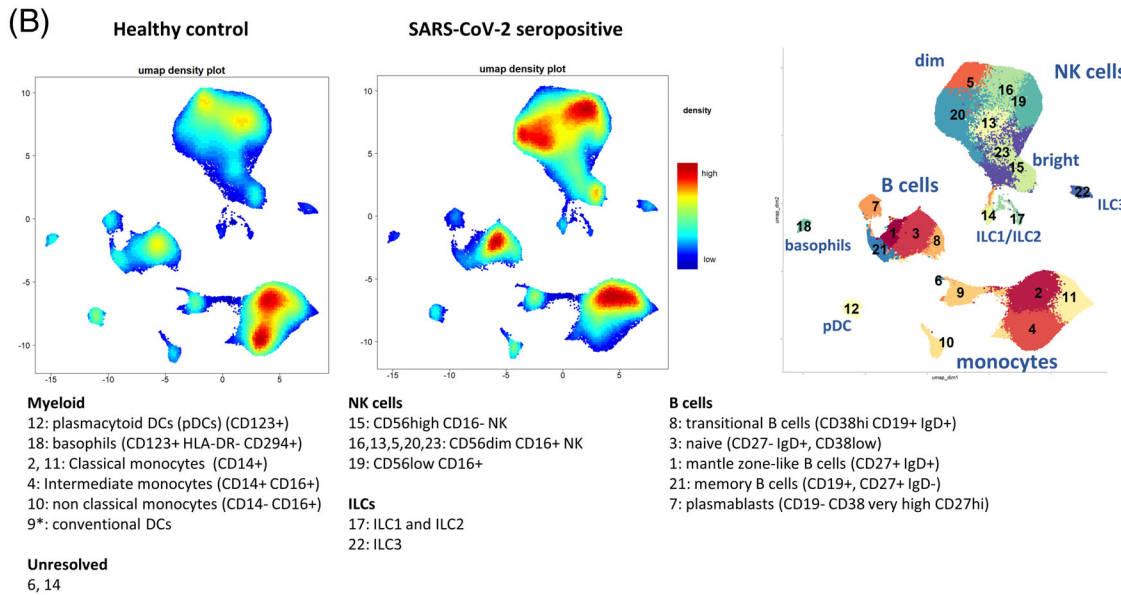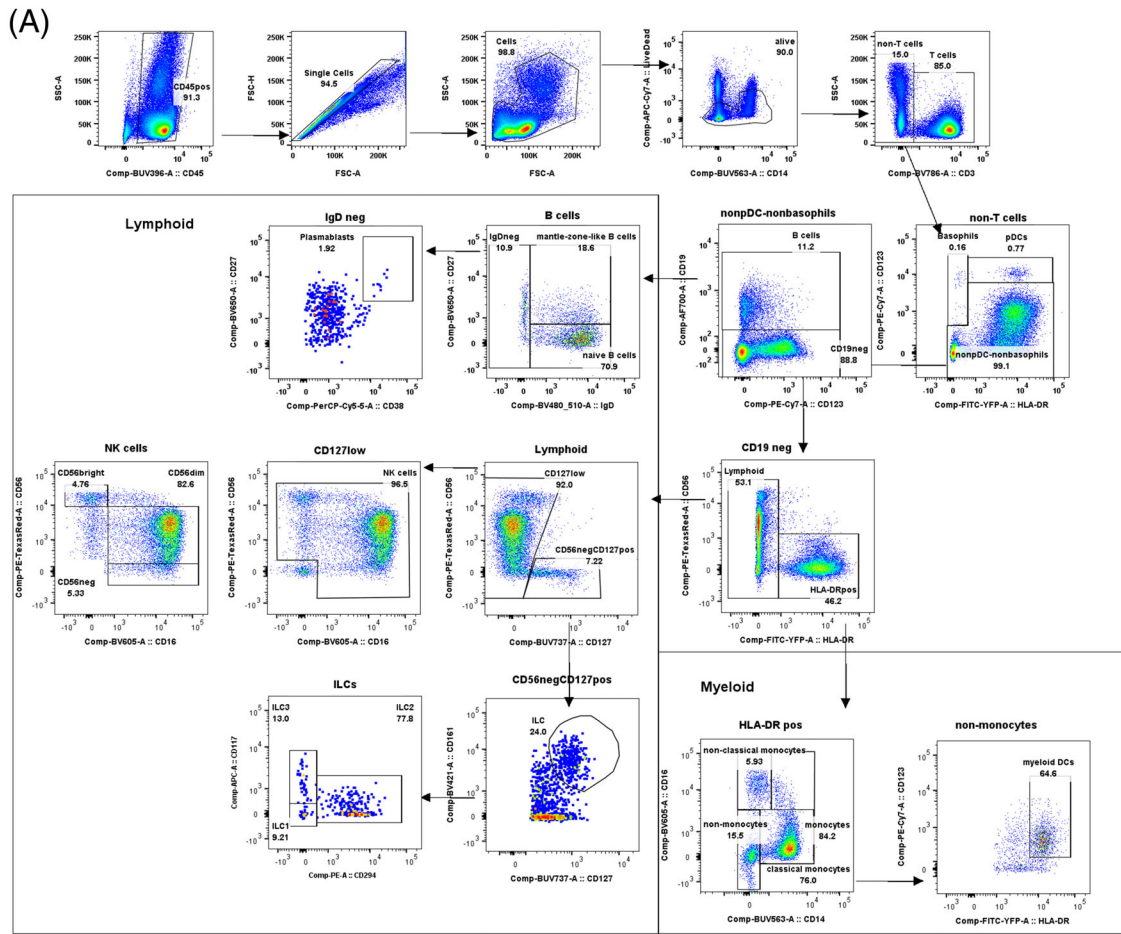
FIGURE 2 Manual gating strategy, and visualization of the unbiased clustering of single-cell multidimensional data for panel B. (A) Sequential gating strategy for B cells and innate immune cells on a representative sample. Names of subpopulations are shown along with frequency within the parent population. The parent population is indicated above the plots or by arrows showing backgating. (B) UMAP analysis of 150,000 live CD45+CD3- cells per group from SARS-CoV-2 seroconverted children compared to age-matched controls. Density plots showing the UMAP analysis for each group. Populations were manually annotated after unbiased clustering; the annotation is shown below the figure. Healthy controls: $n = 5$; SARS-CoV-2 seropositive $n = 7$

these changes could persist long term after COVID-19. In respiratory syncytial virus infection, a reduction in pDC in blood persisted in children for up to 3 months after infection [25].

4 | CONCLUSIONS

Here, we present two flow cytometry panels for an efficient and rapid phenotypic and functional characterization of the pediatric immune response to COVID-19. Both panels perform well in either manual gating or unbiased clustering approaches. Importantly, these panels allow for a broad assessment of the innate and adaptive immune systems, while also identifying small subpopulations with possible relevance in children and SARS-CoV-2 infection, such as ILCs, plasmablasts, recent thymic emigrants, cytotoxic effector CD4+ and CX3CR1+ CD8+ T-cells.

Due to the small number of samples and the relatively long time after infection of this sub-cohort, the differences between healthy and seroconverted children seen in this study should be interpreted with caution and verified in large multi-center studies. The reproducibility of the statistical comparisons obtained using manual and unbiased gating in this work underlines the ability of these panels for robust and quick immune phenotyping in cryopreserved pediatric samples.

We show here that approaches like ours make it possible to generate detailed immunologic data on a broad set of immune cells using relatively small amounts of PBMCs. Furthermore, the selection of markers and optimization of staining protocols for use of cryopreserved pediatric samples presented here could facilitate standardization for multi-center studies. This approach is necessary based on the rarity of severe pediatric COVID-19 and the infrequent Multisystem Inflammatory Syndrome in Children (MIS-C). Conversely, these panels or their adapted variants could be used in the ongoing pandemic as new genetic variants continue to emerge, as well as in future pandemics affecting children.

CONFLICT OF INTEREST
The authors declare no conflicts of interest.

AUTHOR CONTRIBUTIONS
Eva Tolosa and Gabor A. Dunay conceived the study. Thomas S. Mir and Søren W. Gersting were responsible for supervision, funding, and management of the C19.CHILD Hamburg Study cohort. Freya Sibbertsen, Kevin Paul, and Gabor A. Dunay performed the experiments and acquired the data. Freya Sibbertsen, Kevin Paul, Laura Glau, Eva Tolosa, and Gabor A. Dunay analyzed the data and made the figures. Laura Glau performed bioinformatical analysis. Freya Sibbertsen and Laura Glau performed statistical analysis. Freya Sibbertsen and Gabor A. Dunay wrote the first draft of the manuscript. Laura Glau and Eva Tolosa contributed with critical sections to the manuscript. All authors read and critically revised the final version of the manuscript.

PEER REVIEW
The peer review history for this article is available at https://publons.com/publon/10.1002/cyto.a.24528.

ORCID
Freya Sibbertsen https://orcid.org/0000-0001-8907-1582
Kevin Paul https://orcid.org/0000-0002-0998-4881
Thomas S. Mir https://orcid.org/0000-0002-8337-5187
Søren W. Gersting https://orcid.org/0000-0001-7482-4748
Gabor A. Dunay https://orcid.org/0000-0003-0371-1505

REFERENCES
1. Zhou F, Yu T, Du R, Fan G, Liu Y, Liu Z, et al. Clinical course and risk factors for mortality of adult inpatients with COVID-19 in Wuhan, China: A retrospective cohort study. Lancet. 2020;395:1054–62.
2. Dong Y, Mo X, Hu Y, Qi X, Jiang F, Jiang Z. Epidemiological characteristics of 2143 pediatric patients with 2019 Coronavirus disease in China. Pediatrics. 2020;145(6):e20200702.
3. Viner RM, Mytton OT, Bonell C, Melendez-Torres GJ, Ward J, Hudson L, et al. Susceptibility to SARS-CoV-2 infection among children and adolescents compared with adults: A systematic review and meta-analysis. JAMA Pediatr. 2020;175(2):143–156.
4. Cossarizza A, De Biasi S, Guaraldi G, Girardis M, Mussini C. SARS-CoV-2, the virus that causes COVID-19: Cytometry and the new challenge for Global Health. Cyto Part A. 2020;97:340–3.
5. Vella LA, Giles JR, Baxter AE, Oldridge DA, Diorio C, Kuri-Cervantes L, et al. Deep immune profiling of MIS-C demonstrates marked but transient immune activation compared to adult and pediatric COVID-19. Sci Immunol. 2021;6:57.
6. Gruber CN, Patel RS, Trachtman R, Lepow L, Amanat F, Krammer F, et al. Mapping systemic inflammation and antibody responses in multisystem inflammatory syndrome in children (MIS-C). Cell. 2020;183:982–95.
7. Wildner NH, Ahmadi P, Schulte S, Brauneck F, Kohsar M, Lütgehetmann M, et al. B cell analysis in SARS-CoV-2 versus malaria: increased frequencies of plasmablasts and atypical memory B cells in COVID-19. J Leukoc Biol. 2021;109:77–90.
8. Schultheiß C, Paschold L, Simnica D, Mohme M, Willscher E, von Wenserski L, et al. Next-generation sequencing of T and B cell receptor repertoires from COVID-19 patients showed signatures associated with severity of disease. Immunity. 2020;53:442–455.e4.
9. Pauken KE, Godec J, Odorizzi PM, Brown KE, Yates KB, Ngiow SF, et al. The PD-1 pathway regulates development and function of memory CD8+ T cells following respiratory viral infection. Cell Rep. 2020;31:7827.

10. Carter MJ, Fish M, Jennings A, Doores KJ, Wellman P, Seow J, et al. Peripheral immunophenotypes in children with multisystem inflammatory syndrome associated with SARS-CoV-2 infection. Nat Med. 2020;26:1701–7.

11. Chen H, Lau MC, Wong MT, Newell EW, Poidinger M. Cytofkit: A bioconductor package for an integrated mass cytometry data analysis pipeline. PLoS Comput Biol. 2016;12:5112.

12. Poccia F, Agrati C, Castilletti C, Bordi L, Gioia C, Horejsh D, et al. Anti-severe acute respiratory syndrome coronavirus immune responses: the role played by Vγ9Vδ2 T cells. J Infect Dis. 2006;193: 1244–9.

13. Schulze Zur Wiesch J, Thomssen A, Hartjen P, Tóth I, Lehmann C, Meyer-Olson D, et al. Comprehensive analysis of frequency and phenotype of T regulatory cells in HIV infection: CD39 expression of FoxP3+ T regulatory cells correlates with progressive disease. J Virol. 2011;85:1287–97.

14. Fritsch RD, Shen X, Sims GP, Hathcock KS, Hodes RJ, Lipsky PE. Stepwise differentiation of CD4 memory T cells defined by expression of CCR7 and CD27. J Immunol. 2005;175:6489–97.

15. Wang L, Hückelhoven A, Hong J, Jin N, Mani J, Chen B a, et al. Standardization of cryopreserved peripheral blood mononuclear cells through a resting process for clinical immunomonitoring–Development of an algorithm. Cytometry A. 2016;89:246–58.

16. Kohler S, Thiel A. Life after the thymus: CD31+ and CD31 human naive CD4+ T-cell subsets. Blood. 2009;113:769–74.

17. Cossarizza A, Chang HD, Radbruch A, Acs A, Adam D, Adam-Klages S, et al. Guidelines for the use of flow cytometry and cell sorting in immunological studies (second edition). Eu J Immunol. 2019;49:1457–973.

18. Jogdand GM, Mohanty S, Devadas S. Regulators of Tfh cell differentiation. Front Immunol. 2016;7:520.

19. Mahnke YD, Brodie TM, Sallusto F, Roederer M, Lugli E. The who's who of T-cell differentiation: human memory T-cell subsets. Eur J Immunol. 2013;43:2797–809.

20. Gerlach C, Moseman EA, Loughhead SM, Alvarez D, Zwijnenburg AJ, Waanders L, et al. The chemokine receptor CX3CR1 defines three antigen-experienced CD8 T cell subsets with distinct roles in immune surveillance and homeostasis. Immunity. 2016;45:1270–84.

21. Jones TC, Biele G, Mühlemann B, Veith T, Schneider J, Beheim-Schwarzbach J, et al. Estimating infectiousness throughout SARS-CoV-2 infection course. Science. 2021;373(6551):eabi5273. https://doi.org/10.1126/science.abi5273

22. Swieboda D, Guo Y, Sagawe S, Thwaites RS, Nadel S, Openshaw PJM, et al. OMIP-062: a 14-color, 16-antibody panel for Immunophenotyping human innate lymphoid, myeloid and T cells in small volumes of whole blood and pediatric airway samples. Cyto Part A. 2019;95:1231–5.

23. Roan F, Ziegler SF. Human group 1 innate lymphocytes are negative for surface CD3ε but express CD5. Immunity. 2017;46:758–9.

24. Mair F, Liechti T. Comprehensive Phenotyping of human dendritic cells and monocytes. Cyto Part A. 2021;99:231–42.

25. Weng K, Zhang J, Mei X, Wu A, Zhang B, Cai M, et al. Lower number of plasmacytoid dendritic cells in peripheral blood of children with bronchiolitis following respiratory syncytial virus infection. Influ Other Resp Virus. 2014;8:469–73.

SUPPORTING INFORMATION

Additional supporting information may be found in the online version of the article at the publisher's website.